# Permeance based model for the coupled-inductor utilized in the supercapacitor assisted surge absorber (SCASA) and its experimental validation

**Conference Paper** · September 2020

DOI: 10.1109/IESES45645.2020.9210663



**3 authors**, including:

Sadeeshvara Udayanga Silva
University of Canterbury
**15** PUBLICATIONS **9** CITATIONS

SEE PROFILE

# Permeance based model for the coupled-inductor utilized in the supercapacitor assisted surge absorber (SCASA) and its experimental validation

Silva Thotabaddadurage Sadeeshvara Udayanga*, Nihal Kularatna† and D. Alistair Steyn-Ross‡
School of Engineering, University of Waikato, Hamilton, New Zealand
Email: *sus1@students.waikato.ac.nz, {†nihal.kularatna, ‡alistair.steyn-ross}@waikato.ac.nz

***Abstract*—Transient-surge absorption capability of small/low cost supercapacitors (SCs) is already published. SCASA is a patented technique that led to the development of a high performance commercial surge protector which adheres to UL-1449 3rd edition test protocols. The commercial implementation comprises a coupled-inductor, two metal oxide varistors (MOVs) and a SC sub-circuit. This paper presents a permeance based model for the coupled-inductor of SCASA topology in predicting its operation under contrasting voltage conditions. In validating the circuit operation with regard to its surge absorption capability versus 50 Hz AC power transfer, a lightning surge simulator (LSS-6230) was utilized. We discuss this comparison based on the standard IEEE C62.41 surge waveforms up to a maximum of 6.6 kV.**

***Index Terms*—SCASA, Surge absorption, Coupled-inductor, Permeance, Lightning surge simulator**

## I. Introduction

Since the late 19th century to the present day, the demand for electronics has expanded in unimaginable ways. With the modern-day trends towards semiconductor based devices, the mandatory requirement of protecting more sensitive equipment became a necessity [1]. Today, more than 75% of the power generated across the world is processed by power electronics [2]. Processing and conditioning is essential in eliminating power quality issues. In general, various voltage disturbances lower the power quality. In a single- or three-phase utility supply, it is expected that RMS 230 V passes with a minimal tolerance. But, due to unwanted disturbances such as transients, surges, noise and harmonics, the overall condition of power is lowered. A reliable surge protector device (SPD) filters out these transient surges while allowing the uninterrupted passage of utility main. SPDs are basically two types: some directly attenuate (series protection devices) and block the propagation of surge; whereas, in certain cases diversion of the surge (shunt devices) away from the sensitive load becomes very effective in limiting residual voltages. However, all transients and surges are unpredictable and statistical in nature; they can be of many different shapes. In surge protection related studies we refer to the standard surge waveforms defined by the international standards: IEEE C62.41 [3] and IEC 61000-4-5 [4].

In recent past, the power electronics research group at the University of Waikato has tested and highlighted the unique features of supercapacitors (SCs) as applied to surge protection related fields [5]. SCs were originally developed as electrical dual layer capacitors (EDLCs) with million times bigger capacitance than electrolytic capacitors, but typically with a similar size. Having a larger capacitance became advantageous in surge environments as that resulted in million times larger time constants for SCs. This turned out to be a key feature of SCs in order to survive transient surge conditions. Due to the novelty of this application, the patented technology SCASA was originally developed by the University of Waikato, and it was later commercialized as smart TViQ by Thor technologies, Australia [6].

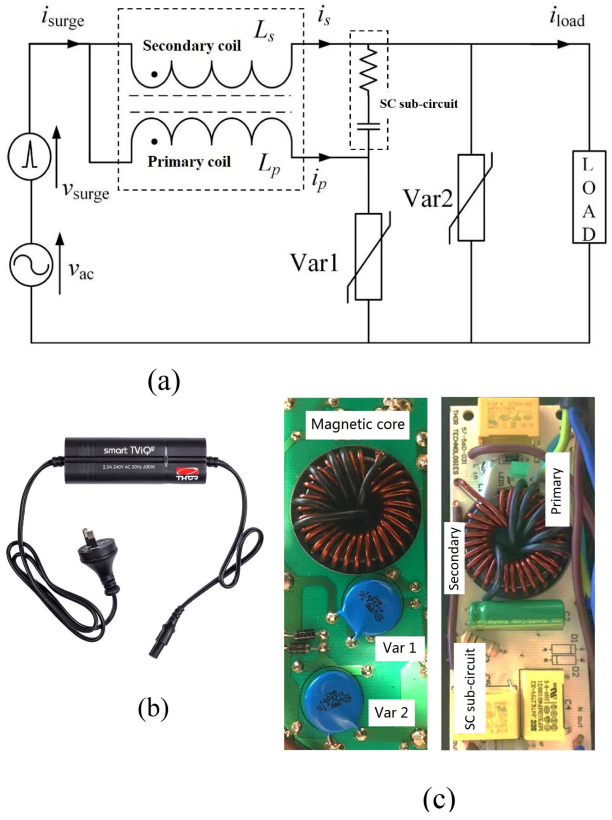


Figure 1. SCASA implementation: (a) circuit topology [7] (b) smart TViQ as a commercial SPD [6] (c) internals of smart TViQ (both sides) [8]

### A. SCASA *design and the coupled-inductor technique*

Following the discovery of SCs' surge-absorption capability [5] to the modern-day product, many challenges were faced by the power electronics team at Waikato; in particular, the

low DC voltage rating of SCs hinders their suitability for circuits working under utility main. Therefore, in developing SCASA technique, a coupled-inductor wound on a powdered-iron toroid is used. By placing a coupled-inductor with two coils of selected number of turns, voltage across the SC is greatly reduced under RMS conditions. In addition, as per the design shown in Fig. 1(a), the two coils partly function as a step-up transformer during the propagation of transient surges. According to the configuration, secondary side of the coupled-inductor induces a higher voltage (greater impedance) than the primary side during a transient event, allowing more transient current to flow through the primary. This effect ensures that minimal surge currents are passed to the load side. Overall, the magnetic action of these two coupled coils protects the critical load as some part of surge energy is getting stored inside the core in terms of flux. Moreover, two metal oxide varistors (MOVs) Var1 and Var2 dissipate the remaining surge energy while maintaining a reliable clamping level to protect the load. More detail about the magnetic action of the core is discussed in section II.

Apart from enhancing the energy storage capacity, coupled-inductor is an effective method used for the implementation of a SC sub-circuit. As previously mentioned SCs have a low voltage rating, hence, in SCASA design a SC is placed between the ends of coupled-inductor coils; this placing ensures the RMS voltage across SC sub-circuit will never exceed the DC rating of SCs. Therefore, any possibilities of damaging the SC is prevented. Fig. 1(a) and 1(c) indicate the placing of a 5 F SC and a 1 $\Omega$ high power resistor. Full explanation regarding RMS operation will be presented in section III (A).

In section III (B), we attempt to examine the transient response of the SCASA core; specially, the transitional effects of current propagations from 50 Hz to surge-frequencies will be analysed. Section IV summarizes the experimental set-up used for the measurement of two main operational modes. Different test conditions and key steps in our methodology are also described under this section. Furthermore, we present and discuss our findings in section V; finally, concluding remarks are given at the end.

## II. Development of models

With the introductory notes about magnetic action, we now focus on investigating the coupled-inductor behaviour in detail. But first it's of greater importance to understand the distribution of frequency components inside a surge pulse.

### A. *Frequency spectrum of a* $1.2/50$ $\mu$s surge pulse

The $1.2/50$ $\mu$s voltage waveform [3] is the standard surge pulse delivered to SPD circuitries; the overall shape of the waveform is governed by a set high frequencies that pushes any SPD to function uniquely compared to 230 V single frequency circumstances.

As shown in Fig. 2, we used LTSpice software tools to obtain the Fourier transform of a 6.6 kV surge waveform; it includes a range of high frequencies starting from below 1 kHz to almost 1 MHz. Here, DC component of the surge has been removed to enhance the spectral representation. Unlike the single frequency AC main (50 Hz), inductive impedances dominate at high frequencies; this effect completely reverses the operation of SCASA design [9]. In section I, we briefly mentioned how the coupled-inductor arms generate different impedances during transient events. However, to further understand the actual propagation of these high frequency components, we need to consider an advanced model of the SCASA transformer core.

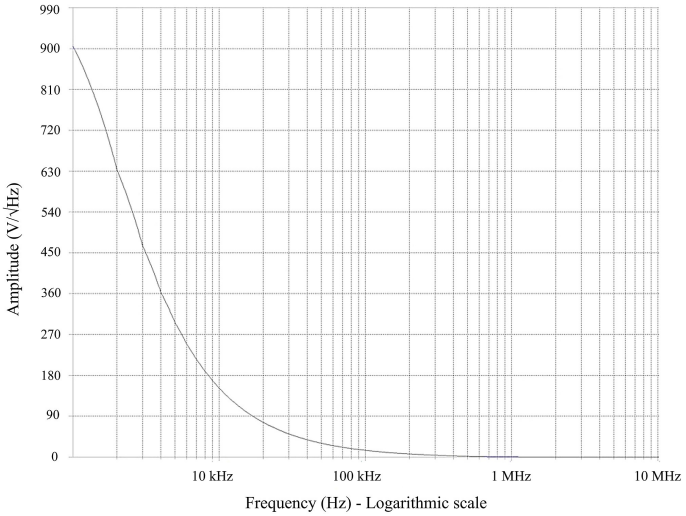


Figure 2. Simulated Fourier transform of a $1.2/50$ $\mu$s surge pulse

### B. *Non-ideal characteristics of the* SCASA *transformer core*

Although the SCASA circuit (Fig. 1) has a simple form, the magnetic core possesses several non-ideal characteristics which cannot be ignored in a fine analysis. Specifically, magnetizing inductances $L_1$ & $L_2$ and leakage inductances $l_1$ & $l_2$ of both primary and secondary windings are of greater relevance to our study (Fig. 3). These non-ideal characteristics push the operation of the transformer core away from ideal behaviour; hence, the currents division across the windings do not occur as per the turns ratio. However, for the accuracy of our model, we replace the ideal core with two windings (Figs. 3 and 4) composed of relevant non-ideal characteristics.

According to the equivalent transformer circuit (Fig. 3) as illustrated below, we can express self inductances of both primary ($L_p$) and secondary ($L_s$) as a series combination of magnetizing and leakage components [10] as indicated by (1) and (2).

A more explicable way of denoting inductance is to use a permeance based model; permeance "$\Lambda$" is defined as the inductance per unit square turns [11]. Hence, we introduce two new parameters named magnetizing permeance $\Lambda_m$ and leakage permeance $\Lambda_\sigma$ as an alternative way of expressing self inductances of the two windings. If $N_1$ and $N_2$ are the respective number of turns of primary and secondary sides, then (1) and (2) can be revised in to (3) and (4). Moreover, magnetic interaction between the two coils is indicated by mutual inductance $M$, and it can be written using $\Lambda_m$ as per

(5). Permeance of the transformer core is closely related to its magnetic reluctance $\mathfrak{R}$ ($\Lambda = 1/\mathfrak{R}$) [12] which provides an obstructing effect for the magnetization and demagnetization processes. In section III, we present a detailed discussion on reluctance in relation to the non-ideality of the core.

Depending on the measurement situation, we can refer secondary side inductive components $L_2$ and $l_2$ to the primary side if needed, by dividing by $n^2$, where $n = N_2/N_1$ is the secondary:primary turns ratio of the windings [13]. Then, we can express the total effective inductance $L_p{}'$ seen by the primary according to (6). Conversely, (7) specifies the total effective inductance seen by the secondary. Here, we have omitted the copper losses and core losses as their impact to this analysis is negligible.

$$L_p = L_1 + l_1 \tag{1}$$

$$L_s = L_2 + l_2 \tag{2}$$

$$L_p = \Lambda_m {N_1}^2 + \Lambda_\sigma {N_1}^2 \tag{3}$$

$$L_s = \Lambda_m {N_2}^2 + \Lambda_\sigma {N_2}^2 \tag{4}$$

$$M = \Lambda_m N_1 N_2 \tag{5}$$

$$L_p{}' = L_1 + l_1 + L_2/n^2 + l_2/n^2 \tag{6}$$

$$L_s{}' = L_2 + l_2 + L_1 \cdot n^2 + l_1 \cdot n^2 \tag{7}$$

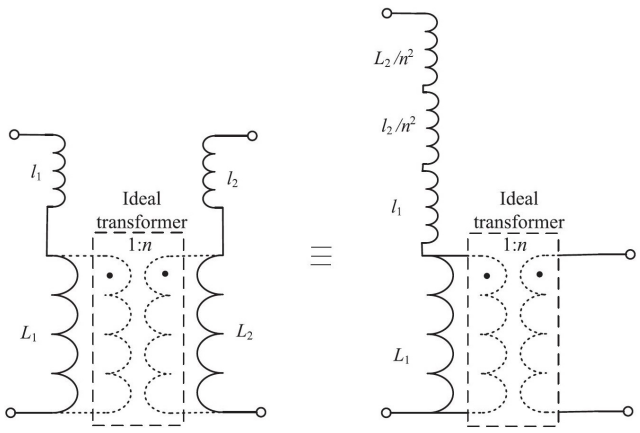


Figure 3. Equivalent circuit of the non-ideal transformer core of SCASA design

Since SCASA transformer core utilizes a toroid made of powdered-iron, leakage inductance arises from two main sources. Winding configuration of the coils and inner diameter of the toroid are the key factors affecting flux leakage in this situation [14]. On the other hand, magnetizing inductance reflects the overall magnetic properties of the material; softness/hardness of the material and the ability to generate and sustain a magnetic flux are the decisive factors here [15]- [16].

## III. Operational modes of the coupled inductor

With the model presented above, we now aim at investigating the 50 Hz AC operation and surge response of SCASA circuit in a detailed manner. Here, we must consider the fact that two transformer coils are coupled under all voltage circumstances. Unlike a conventional transformer, in this case, currents are shared among primary and secondary sides depending on their impedance levels at different conditions.

### A. AC *operation*

Under 230 V AC, neither of the varistors Var 1 and Var 2 are fired; hence, they do not conduct currents as MOVs have mega ohms level resistances during non-conduction phase. In Fig. 4, we indicate these open-circuit conditions using dotted lines, and under such conditions RMS currents only pass through the two inductor arms.

Considering both resistive and reactive elements, it is possible to determine the total impedance in the primary path as,

$$Z_1 = R + j\omega L_1 + j\omega l_1 + \frac{1}{j\omega C} \tag{8}$$

Similarly, the total impedance in the secondary can be expressed as a sum of two inductive reactances:

$$Z_2 = j\omega L_2 + j\omega l_2 \tag{9}$$

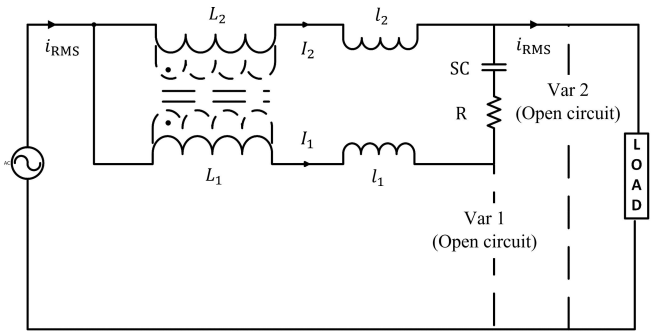


Figure 4. 50 Hz AC operation of the non-ideal transformer core

Now that, by putting a high current device (electric iron) across the load terminals, it is possible to measure how RMS currents are shared between the two coils. It is recognizable that the total RMS current through the load is the sum of individual currents in both primary and secondary (as varistors are in non-conduction mode). Compared to the high frequency components of a surge (Fig. 2), 50 Hz is a less significant value. Therefore, with the $\mu$H level inductive coils wound to the SCASA core, we can predict that 50 Hz based inductive-impedances are fairly insignificant. As a result, it is expected to have a major current flow in secondary side of the core. Here, SCASA circuit is directly connected to the 230 V utility main whereas a load of 1200 W (electric iron) is plugged to the output side. In section V, we include clamp-meter based test results (Table I) to justify our prediction.

### B. Transient operation

Here, we emphasize how the coupled-inductor of the SCASA transformer switches operation from 50 Hz AC to transient conditions. Under high voltage conditions, both Var 1 and Var 2 exceed their breakdown points; hence, enter into their conduction phases. Then, the open circuit conditions (dashed lines) illustrated in Fig. 4 must be replaced with appropriate "ON resistances" ($R_{ON}$). According to the varistor model [17] of V20E275 (UltraMOV Series-Littlefuse) utilized in SCASA circuit, ON resistances of both Var1 and Var2 is about 7.5 Ω [18].

Modelling the transient propagation becomes a complex task specially with the continuous spectrum of frequencies (Fig. 2); unlike the case of 50 Hz AC, here, we expect to see a distribution of impedances associated with each frequency component. Laplace transform based analysis will yield analytical solutions to accurately predict the propagation of currents. We think a detailed mathematical analysis is beyond the scope of this paper; however, we can write down the relevant Kirchhoff's equations for voltage divisions as follows:

$$V_{surge}(s) = \tilde{I}_1(s)\big[sL_1 + sl_1\big] + \big[\tilde{I}_1(s) + \tilde{I}_2(s)\big].R_{ON} \quad (10)$$

where $\tilde{I}_1(s)$ and $\tilde{I}_2(s)$ are the $s$-domain surge currents in both primary and secondary respectively; while the normalized Laplace representation of the surge pulse is indicated by $V_{surge}(s)$. Considering the simplicity, (10) is written for an open-circuit SCASA without the second varistor.

If we consider the closed loop around coupled-inductor with the SC sub-circuit (Fig. 4), it is possible to obtain another relationship between $\tilde{I}_1(s)$ and $\tilde{I}_2(s)$:

$$\tilde{I}_2(s)\big[sL_2 + sl_2 + \frac{1}{sC} + R\big] - \tilde{I}_1(s)\big[sL_1 + sl_1\big] = 0 \quad (11)$$

The most noticeable aspect in transient operation is the reversing effect of current flows. Under high frequencies, inductive impedances dominate; therefore, the more inductive secondary side gets the least amount of currents while substantial portion of surge current passes to Var1 through the primary side. Here, we do not attempt to provide analytical solutions to (10) and (11); but, we now delve into magnetic reluctance of the non-ideal SCASA core to see why the ratio of transient currents ($i_1/i_2$) does not satisfy the inverse ratio ($N_2/N_1$) of number of turns.

In the previous section, it became clear to us that the coupled-inductor core does not behave ideally as expected; basically a transformer must operate according to its turns ratio unless affected by magnetic reluctance of the core material. In an ideal case, the Ampere's law yields the following relationship (12) between primary and secondary currents.

$$N_1 i_1 + N_2 i_2 = 0 \quad (12)$$

Since SCASA utilizes a powdered-iron toroid, the air-bubbles distributed inside the core material make the medium more reluctive to the formation of magnetic flux. This extra reluctance modifies (12) into (13) as below [19]:

$$N_1 i_1 + N_2 i_2 = \Phi\Re \quad (13)$$

where $\Phi$ is the net magnetic flux through the toroidal core of SCASA during transient operation. Equation (13) can be rearranged into:

$$i_1 = \frac{\Phi\Re}{N_1} - \frac{N_2}{N_1}\, i_2 \quad (14)$$

This result clearly indicates why SCASA's coupled-inductor arms do not share currents as an ideal transformer. This study further revealed us that non-ideal behaviour of the core is highly significant specially during the propagation of transient currents. We look forward to bring this discussion further into section V to compare the compatibility of our theoretical approach with experimental findings.

## IV. Experimental Setup

To verify the two operational modes, we tested SCASA devices under contrasting conditions. Fig. 5 demonstrates the test setup used to validate AC current propagation. Here, 230 V utility main is directly passed to the SCASA unit via the LSS, whereas a high current device (1200W electric iron) is connected to the load side.

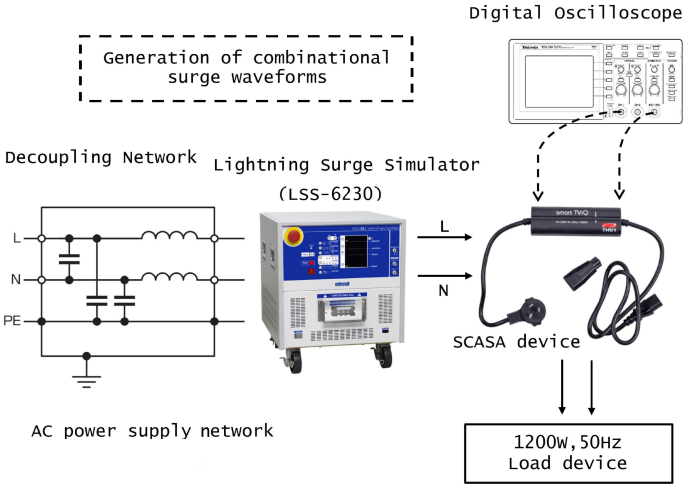


Figure 5. Experimental setup for measuring AC and transient operations

Two coupled-inductor coils inside the SCASA transformer were separately clamped using a clamp meter (TEKTRONIX A622) to observe the sharing of currents. In section V, we discuss RMS current measurements and different test conditions considered (Table I).

A lightning surge simulator (NoisenKen LSS-6230) and a digital oscilloscope (Tektronix TPS2014) were the key instruments used for the observation of transient operation (Fig. 5). Decoupling network ensures that none of the injected surge pulses are going to flow back to the utility main. Moreover, an isolation transformer was inserted between LSS and wall socket as a safety precaution. Surge currents propagation

through the core was indirectly measured by capturing the variations of voltages across externally inserted resistors (Table II).

Here, different magnitudes of 1.2/50 µs surge pulses were generated using the LSS-6230; thus, oscilloscope waveforms (Fig. 6) were recorded for 3.3 kV and 6.6 kV peak voltages.

## V. Test Results and Discussion

Test results obtained for both AC and transient operations showed good compatibility with our modelling approach. As predicted in section III (A), we measured nearly 95% (CH1) of the RMS current flow in secondary; whereas only 5% (CH2) passed through the primary coil (Fig. 6(a)/Table I). All currents were measured as RMS values; the total RMS current drawn from the wall socket was expected to be ∼5 A for the 1200 W load. For a better accuracy, measurements were repeated for 120 V as well. Table I summarizes all clamp-meter based measurements.

Table I
Comparison of Primary and Secondary RMS Currents During 50 Hz AC Operation

| Test Condition | Voltage $V_{RMS}$ (V) | Primary coil current $I_1$(A) (RMS) | Secondary coil current $I_2$(A) (RMS) | Measured total current $I_{RMS}$(A) |
|---|---|---|---|---|
| SCASA + IRON | 230 | 0.15 | 4.81 | 5.04 |
| SCASA + IRON | 120 | 0.12 | 2.61 | 2.64 |
| IRON | 230 | - | - | 5.08 |
| IRON | 120 | - | - | 2.64 |

Table II
Comparison of Primary and Secondary Peak Currents During Transient Operation

| Test Condition | Peak Surge Voltage $V_{surge}$ (V) (CH4) | Peak Surge Current $i_{surge}$ (A) (CH3) | Primary peak current $i_1$(A) (CH1/0.21) | Secondary peak current $i_2$(A) (CH2/0.21) |
|---|---|---|---|---|
| 1.2/50 µs surge pulse | 3.3 kV | 1380 | 914.3 | 476.2 |
| 1.2/50 µs surge pulse | 6.6 kV | 2940 | 1790.5 | 1142.8 |

We considered four main test conditions under 50 Hz AC operation; total RMS currents were measured with and without SCASA device for two voltage conditions: 120 V and 230 V. The main reason behind such an attempt was to understand the impact of SCASA circuit on AC main propagation. As highlighted in Table I, the reduction of $I_{RMS}$ in the presence of SCASA device is almost negligible (5.08 A → 5.04 A); noticeably, this observation is true for both voltage conditions.

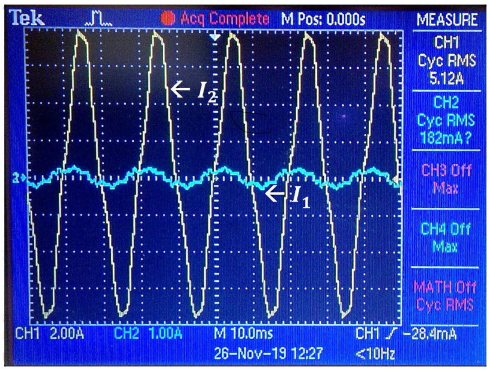


(a)

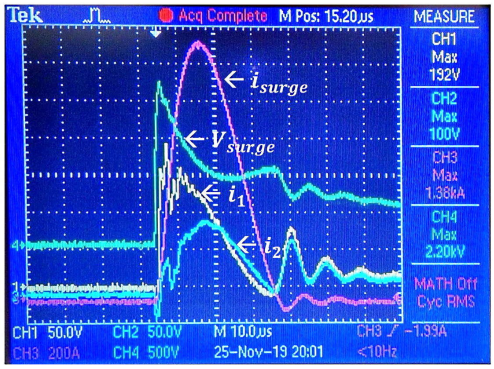


(b)

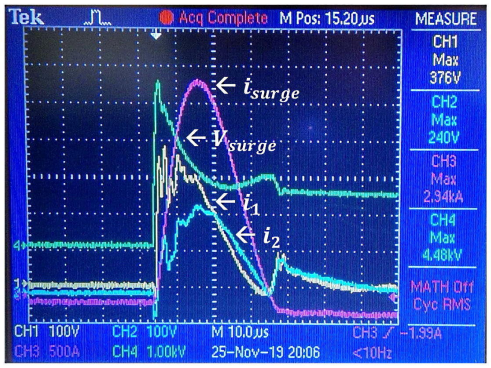


(c)

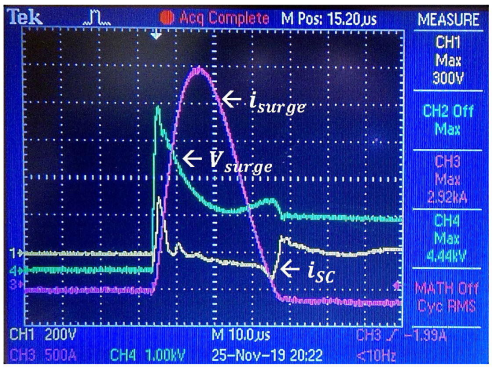


(d)

Figure 6. Oscilloscope waveforms for different operational modes: (a) AC operation (230 V) (b) Transient operation (3.3 kV) (c) Transient operation (6.6 kV) (d) SC sub-circuit current (6.6 kV)

In observing transient operation, oscilloscope waveforms captured for voltage variations indirectly gave us information about currents through the coupled-inductor coils. Here we placed a parallel combination of five 1 Ω high-power resistors (0.21 Ω) across the primary and secondary sides of SCASA transformer core, and captured the voltage variations across them. Then, these peak voltage values were divided by 0.21 Ω to find the corresponding peak surge currents (Table II). Even though this method yields slightly diminished current values, the ratio between transient currents ($i_1/i_2$) stays the same. Thereby, we can identify the percentages of $i_{surge}$ shared among both coils. According to Fig. 6(b) and 6(c), it is clear that $\sim$ 62% (CH1) total surge current propagates through the primary, whereas only $\sim$ 38% (CH2) flows through the secondary. This distinctly is a contrasting transition from the 50 Hz RMS operation.

However, it is understandable that above percentages are not in reciprocal agreement with the turns ratio ($\frac{N_2}{N_1} = 28/6$). In (13) we explained this discrepancy is due to the magnetic reluctance caused by the powdered-iron toroid. Using manufacturer's specifications [20] for magnetizing permeance $\Lambda_m$ ($61 \times 10^{-9}$ H) [21], it is possible to quantify the core reluctance as previously discussed ($\Re = \frac{1}{\Lambda_m} = 1.64 \times 10^7$ A. turns/Wb). By knowing the magnitudes of $i_1$ and $i_2$ (Table II), we can empirically confirm the accuracy of (13). Note that for the calculation of maximum possible flux $\Phi_{max}$ through the core, we assume a no load condition in which total surge current $i_{surge}$ passes completely through the primary [22]. This gives us a good approximation for the possible peak flux ($1.098 \times 10^{-3}$ Wb) even when a load is functioning at the SCASA's output end.

Moreover, Fig. 6(d) illustrates the flow of transient currents into the SC sub-circuit ($i_{SC}$). This reveals approximately $\sim$10% (CH1) of $i_{surge}$ is passing on to SC; it's fairly insignificant under these circumstances. For this measurement system, insertion of external resistors were not required as the SCASA circuit itself has a 1 Ω high-power resistor; thus, voltage variation across that is as same as the current variation. However, depending on this situation, we can argue that entire secondary current $i_2$ and nearly $\sim$16% of $i_1$ is flowing into Var2 which is very likely with the breaking down of Var2. Under such sharing of currents, it is clear that Var1 gets most of $i_{surge}$ as $i_1$ is significantly greater than $i_2$.

## VI. Conclusion

In this research, we have presented a permeance-based model for the coupled-inductor/transformer core of SCASA technique. Various non-ideal characteristics associated with the two windings were identified, and the main operational modes of the core were discussed in detail. As the core is composed of a powdered-iron toroid, we found that the effects of magnetic reluctance and leakages are non-negligible; hence, these matters were addressed in our analytical work. Experimentation primarily consisted of two phases: measurement of AC operation and detection of surge current propagation. Under both these circumstances, results obtained showed a clear agreement with analytical predictions. This further justified how the core switches between the two operational modes. As a verification step of transient response, we tested the sharing of currents in two transformer coils for the maximum capable 6.6 kV and 3.3 kV surge waveforms. In future research work, we aim to extend our analysis with solutions to the Laplace transform based equations mentioned in section III.

## References


[1] The International Technology Roadmap for Semiconductors 2.0: (ITRS 2.0), European Semiconductor Industry Association, Executive summary report, 2015.

[2] N. Kularatna, "Power Electronics Design Handbook", Elsevier-Newnes, Burlington, MA, 2006.

[3] IEEE Standard C62.41.2, "IEEE Recommended Practice on Characterization of Surges in LowVoltage (1000 V and Less) AC Power Circuits", 2002, pp. 1–85.

[4] "IEC 61000-4-5 Standard Overview: ST Micro electronics", St.com, 2013. [Online]. Available at: https://www.st.com/content/ccc/resource/technical/document/application-note/. [Accessed: 18-Nov-2018].

[5] N. Kularatna, J. Fernando, S. James, A. Pandey, "Surge capability testing of supercapacitor families using a lightning surge simulator", IEEE transactions on Industrial Electronics, 2011, pp. 4942-4949.

[6] Thor Technologies, "STViQ/3 SMART TViQ," 2018. [Online]. Available: https://www.thortechnologies.com.au/product/stviq3/. [Accessed: 22-Nov-2019].

[7] J. Fernando, Supercapacitor-Assisted Surge Absorber (SCASA) and Supercapacitor Surge Modelling (Doctoral thesis), School of Engineering, The University of Waikato, 2016.

[8] S. T. Sadeeshvara Udayanga, N. Kularatna and D. A. Steyn-Ross, "Investigating the impact of ferrite magnetic cores on the performance of supercapacitor assisted surge absorber (SCASA) technique," 2019 IEEE 28th International Symposium on Industrial Electronics (ISIE), Vancouver, BC, Canada, 2019, pp. 130-135.

[9] N. Kularatna, A. Steyn Ross, J. Fernando, S. James, "Design of Transient Protection Systems", Elsevier, 2019, pp 160-171.

[10] A. Bossche and V. Valchev, Inductors and transformers for power electronics. New York: Taylor & Francis, 2005, pp 24-54.

[11] C. MacLyman, "Transformer and inductor design handbook". New York: Dekker, 1978, pp 05-45.

[12] A. Bossche and V. Valchev, Inductors and transformers for power electronics. New York: Taylor & Francis, 2005, pp 01-20.

[13] Massimo Ceraolo; Davide Poli, "Magnetic Circuits and Transformers," in Fundamentals of Electric Power Engineering: From Electromagnetics to Power Systems, IEEE, 2014, pp.215-238

[14] Magnetics - Powder Core Documents, Mag-inc.com, 2018. [Online]. Available: https://www.mag-inc.com/Design/Technical-Documents/Powder-Core-Documents. [Accessed: 06- Nov- 2019].

[15] B. D. Cullity; C. D. Graham, "Soft Magnetic Materials," in Introduction to Magnetic Materials , , IEEE, 2009, pp. 439-476.

[16] B. D. Cullity; C. D. Graham, "Hard Magnetic Materials," in Introduction to Magnetic Materials , , IEEE, 2009, pp. 477-504.

[17] Littlefuse, "Varistor SPICE Models", Littlefuse.com, 2003. [Online]. Available at: http://www.littelfuse.com/technicalresources/spice-models/varistor-spice -models.aspx, [Accessed: 05- May- 2018].

[18] S. James, N. Kularatna, A. Steyn-Ross, R. K€unnemeyer, "Estimation of transient surge energy transferred with associated time delays for individual components of surge protector circuits", IET Power Electron. 8 (5), 2015, pp. 685–692.

[19] S.V.Marshall, R.E. DuBoff, and G.G. Skitek, "Electromagnetic Concepts and Applications", Prentice Hall, Upper Saddle River, NJ, 1996, pp. 101–446.

[20] "Magnetics - Kool Mu Powder Cores", Mag-inc.com, 2018. [Online]. Available at: https://www.mag-inc.com/products/powder-cores/kool-mu-cores. [Accessed: 22- Nov- 2019].

[21] J. Fernando, Supercapacitor-Assisted Surge Absorber (SCASA) and Supercapacitor Surge Modelling (Doctoral thesis), School of Engineering, The University of Waikato, 2016, pp. 77

[22] N. Kularatna, A. Steyn Ross, J. Fernando, S. James, "Design of Transient Protection Systems", Elsevier, 2019, pp 157.